



## Article

# Remote Sensing Identification and Spatiotemporal Change Analysis of *Cladophora* with Different Morphologies

Wenting Xu <sup>1,2,3</sup>, Qian Shen <sup>2,3,\*</sup>, Bo Zhang <sup>1</sup>, Yue Yao <sup>2,3</sup> , Yuting Zhou <sup>2,3,4</sup>, Jiarui Shi <sup>2,3</sup>, Zhijun Zhang <sup>5</sup>, Liwei Li <sup>2,3</sup> and Junsheng Li <sup>2,3,6</sup>

- <sup>1</sup> College of Geography and Environmental Science, Northwest Normal University, Lanzhou 730030, China; 2021120198@nwnu.edu.cn (W.X.)
- <sup>2</sup> Key Laboratory of Digital Earth Science, Aerospace Information Research Institute, Chinese Academy of Sciences, Beijing 100094, China
- <sup>3</sup> International Research Center of Big Data for Sustainable Development Goals, Beijing 100094, China
- <sup>4</sup> School of Marine Technology and Geomatics, Jiangsu Ocean University, Lianyungang 222000, China
- <sup>5</sup> Monitoring Department, Qinghai Eco-Environment Monitoring Center, Xining 810000, China
- <sup>6</sup> School of Electronic, Electrical and Communication Engineering, University of Chinese Academy of Sciences, Beijing 100049, China
- \* Correspondence: shenqian@radi.ac.cn

**Abstract:** *Cladophora qinghaiensis*, an endemic species of *Cladophora* in saltwater lakes, was scientifically named in 2021 (hereafter referred to as *Cladophora*). *Cladophora* exists in different morphologies, including attached submerged *Cladophora* (AC), grown floating *Cladophora* (GFC), and death floating *Cladophora* (DFC). Previous satellite remote sensing has mainly focused on identifying floating algae. In this study, Qinghai Lake served as a case study, and a classification decision tree model (CDTM) was proposed. The model employed the chlorophyll spectral index (CSI) and the normalized difference vegetation index (NDVI) to differentiate AC, Floating *Cladophora* (FC), and water. Additionally, the floating *Cladophora* index (FCI) was introduced to further distinguish GFC and DFC within FC. The method was applicable to Sentinel-2 images from 2016–2023. Visual interpretation methods were used for Landsat series images from the summer months (July to September) to obtain the AC and FC. The results demonstrate that over the past 30 years, the areas inhabited by AC and FC have increased gradually. The three morphologies of *Cladophora* also exhibited seasonal variations, with growth observed annually in May–June, reaching peaks in August–September, and gradually declining in October. In addition, by combining factors such as water surface area and climatic factors, we analyzed the driving forces influencing the changes in *Cladophora*. In this research, AC and FC showed significant correlations with the water surface area, with correlation coefficients ( $r$ ) of approximately 0.9 and 0.7, respectively. These new findings provide valuable insights regarding the spatiotemporal changes and underlying causes for different morphologies of *Cladophora* in global saline lakes.

**Keywords:** filamentous algae; Qinghai Lake; Sentinel-2; driving force; climatic factors



**Citation:** Xu, W.; Shen, Q.; Zhang, B.; Yao, Y.; Zhou, Y.; Shi, J.; Zhang, Z.; Li, L.; Li, J. Remote Sensing Identification and Spatiotemporal Change Analysis of *Cladophora* with Different Morphologies. *Remote Sens.* **2024**, *16*, 602. <https://doi.org/10.3390/rs16030602>

Academic Editor: Teodosio Lacava

Received: 4 January 2024

Revised: 29 January 2024

Accepted: 2 February 2024

Published: 5 February 2024



**Copyright:** © 2024 by the authors. Licensee MDPI, Basel, Switzerland. This article is an open access article distributed under the terms and conditions of the Creative Commons Attribution (CC BY) license (<https://creativecommons.org/licenses/by/4.0/>).

## 1. Introduction

Algal blooms are occurring frequently in numerous oceans and freshwaters worldwide [1–11]. This phenomenon has certain economic and ecological impacts [12,13]. Traditional sampling methods are expensive, inefficient, and labor-intensive, yet fail to obtain crucial information regarding the causes of these algal outbreaks. Satellite remote sensing data can be used to mitigate these issues owing to their wide range, cost-effectiveness, and periodicity [14]. At present, this type of data has been used to extract the area, degree, and duration of algal outbreaks through spectral indices and classification methodologies [4,15–23]. Additionally, visual interpretation has been widely employed to obtain increasingly precise information about algal blooms within a region [6,24–27].

*Cladophora qinghaiensis* is an opportunistic and filamentous alga that thrives in saline lakes [28]. *Cladophora* blooms are the most frequent in these lakes, particularly in Qinghai Lake [29–33]. To adapt to the unique ecological environment of saline lakes like Qinghai Lake, *Cladophora* exhibits different morphologies such as the attached and floating morphologies [28,30,34]. Previous studies have focused mostly on remote sensing identification of algae with singular morphologies [4,6,15–23]. Comparatively less attention has been paid to algae with both floating and attached morphologies, owing to the high degree of difficulty in identifying or distinguishing between them. Some scholars assume that the spatial distribution of floating and attached algae does not overlap, and use the prior knowledge of phenological differences among different morphological algae or aquatic vegetation. These researchers have mapped the distribution areas of different morphological algae or aquatic vegetation [35,36]. However, this assumption largely relies on prior knowledge and may not be applicable to identifying different morphological algae in other lakes. Aquatic vegetation and algae share certain optical characteristics. Some scholars have used trial and error, visual inspection, the classification decision tree model, or spectral indices to identify different forms of aquatic vegetation [21,27,37–43]. Compared with the remote sensing-based identification of the different morphologies of other algae or aquatic vegetation, the remote sensing research of *Cladophora* has lagged. Moreover, research has mainly focused on the remote sensing identification of floating *Cladophora* and analyses of its influencing factors [32,33,44,45]. Knowledge of the recognition methods for different morphologies of *Cladophora* is still lacking.

Based on previous field experimental data collection and document research, the *Cladophora* morphologies include: attached submerged *Cladophora* (AC), grown floating *Cladophora* (GFC), and death floating *Cladophora* (DFC) [46,47]. To comprehensively detail the variations and growth causes of the different morphologies of *Cladophora*, we integrated multi-source optical remote sensing images, constructed or utilized remote sensing identification methods, obtained the distribution area of different morphologies of *Cladophora* from 1990 to 2023, and analyzed the spatiotemporal distribution characteristics of *Cladophora* in different morphologies. Based on this approach, in conjunction with influencing factors such as water surface area and climatic factors, we elucidate crucial concepts; examples include the growing rule and the factors influencing *Cladophora* spread.

## 2. Materials

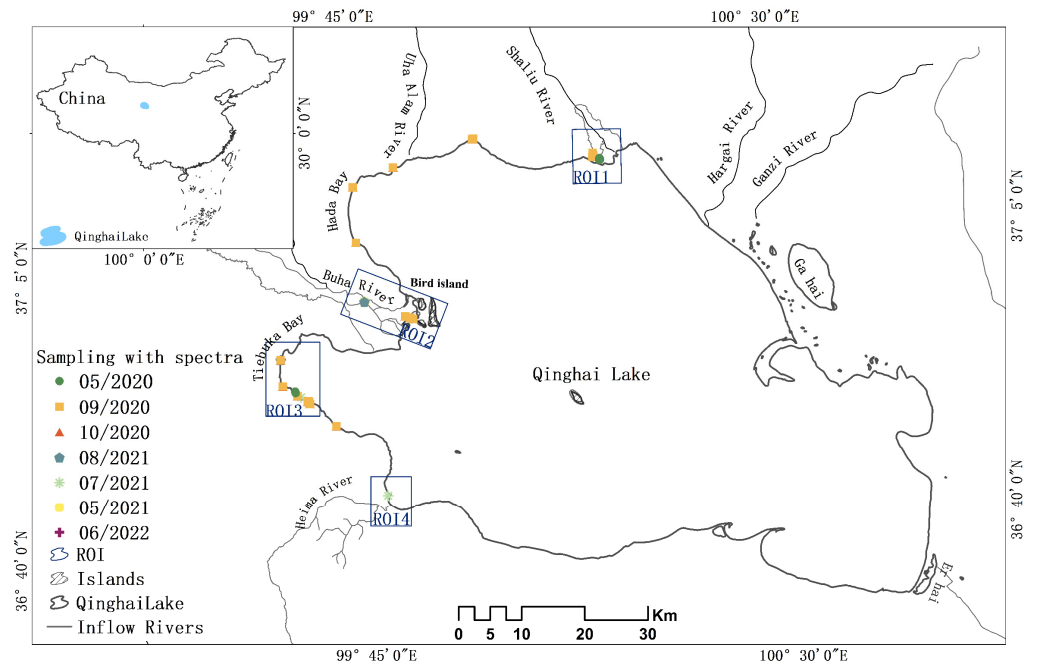
### 2.1. Study Area

Qinghai Lake is the most extensive inland plateau closed lake with salty water in China, in which the areas with more frequent *Cladophora* occurrences are predominantly within the gray range of Figure 1 [30,32]. The study area (latitude 36°35′–37°20′N; longitude 99°35′–100°20′E) is shown in Figure 1. These lake bays and river inlets are represented by the regions enclosed in blue rectangles. The regions of interest (ROI) are defined as follows: ROI 1 is the Shaliu River inlet, ROI 2 is the Buha River inlet, ROI 3 is Tiebuka Bay, and ROI 4 is the Heima River inlet. The island, known as Bird Island, is situated within the boundaries of the ROI 2 rectangle.

### 2.2. Data Source

#### 2.2.1. Measured Data

Field experiments were conducted during May, September, and October 2020, July and August 2021, and June 2022, for a total of seven experiments. We sampled 106 field points with 22, 32, 21, 2, 5, 9 and 15 field points in those experiments, respectively. At each field point, we observed that the FC exists directly above the AC, FC including GFC or DFC. The field reflectance spectra of related objects (AC, GFC, DFC, and water), and the data of each site (GPS position and photos) were recorded. A Field-SpecR3 spectroradiometer and ATP9100 spectroradiometer were used to measure in situ reflectance spectra.



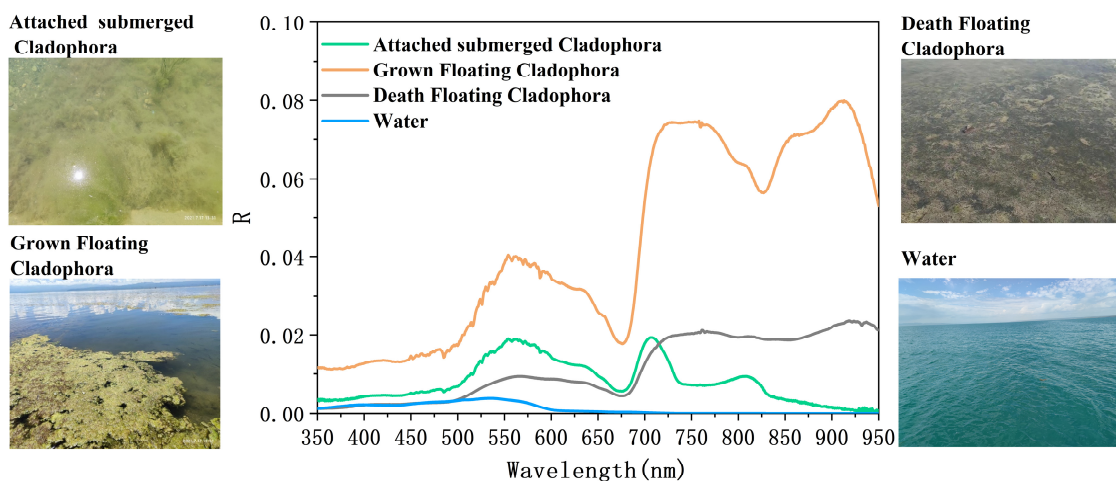
**Figure 1.** The locations of field investigation samples collected from 2020 to 2022.

The in situ reflectance spectral data for AC, GFC, DFC and water were obtained by directly measuring the object reflectance  $R$  (Equation (1)).

$$R(\lambda) = \frac{E_u(\lambda)}{E_d(\lambda)} \tag{1}$$

where  $E_u(\lambda)$  refers to the upward irradiance of the water surface.  $E_d(\lambda)$  refers to the downward irradiance the water surface.

We analyzed 30 spectra at each sampling point, removed outliers, and averaged the remaining spectral reflectance values to obtain the mean reflectance spectra for AC, GFC, DFC, and water (Figure 2).

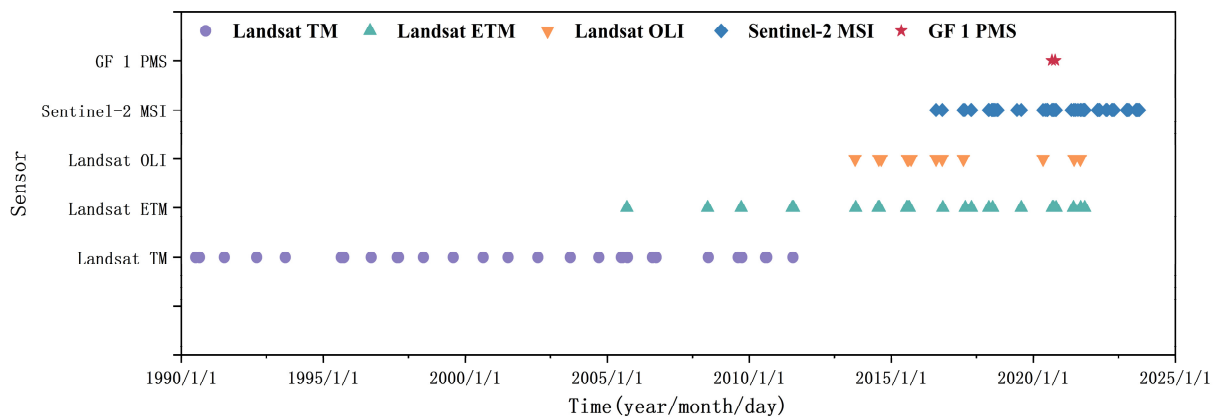


**Figure 2.** The mean reflective spectra of AC, GFC, DFC, and water.

In addition, to investigate the climatic factors that affect *Cladophora* changes, daily climatic factors from 1990 to 2022, including temperature, precipitation, sunshine duration, and wind speed, were selected for Guncha and Gonghe counties.

## 2.2.2. Remote Sensing Images

We collected 262 remote sensing images covering the study area during in non-glacial and less cloudy periods. These primarily included Thematic Mapper (TM), Enhanced Thematic Mapper (ETM), and Operational Land Imager (OLI) images from the Landsat series during the summers of 1990–2021 (July to September). Additionally, Sentinel Multi-Spectral Imager (MSI) images from April 2016 to October 2023 were incorporated (Figure 3). We further validated and evaluated the accuracy of other satellite data in *Cladophora* identification using high-resolution remote sensing images. High-resolution remote sensing images were from the Chinese Gaofen-1 (GF 1) panchromatic multispectral sensor (PMS). From 2016 to 2023, Sentinel-2, Landsat series images and GF PMS images provided effective data, we selected all non-glacial Sentinel-2 images which are known for their higher spatial and temporal resolution, to identify different morphologies of *Cladophora*, and then Landsat series images and GF PMS images were used for validation. From 1990 to 2015, the Landsat series images during the summer months (July to September) were selected to identify different morphologies of *Cladophora*.



**Figure 3.** Time series of remote sensing images.

## 3. Methods

### 3.1. Remote Sensing Data Preprocessing

To ensure the geographic accuracy and consistency of remote sensing images, preprocessing remote sensing images was necessary. Level-1C (L1C) Sentinel-2 images were downloaded from the European Space Agency (ESA) data-sharing website. First, the L1C data were atmospherically corrected using Sen2cor v2.9 software provided by the ESA to obtain Level-2A (L2A) surface reflectance data. Second, because Qinghai Lake was positioned at the junction of the four Sentinel-2 images, cloudless images on the same day were resampled and mosaicked together using the Sentinel Application Platform (SNAP) v9.0 as recommended by the ESA.

In order to use Sentinel-2 to construct CDTM to identify the three forms of *Cladophora*, we first need to simulate the reflectance  $R_{eq}$  of each band's equivalent to those of the images according to the measured reflectance spectra of AC, GFC, DFC, and water in the field, and utilize the spectral response functions of Sentinel-2 MSI remote sensing images, as shown in Equation (2):

$$R_{eq} = \frac{\int R(\lambda) f_{SRF}(\lambda) F_0(\lambda) d(\lambda)}{\int f_{SRF}(\lambda) F_0(\lambda) d(\lambda)} \quad (2)$$

where  $R_{eq}$  refers to the satellite band equivalent reflectance,  $R(\lambda)$  refers to the measured remote sensing reflectance,  $f_{SRF}(\lambda)$  refers to the spectral response function of the satellite, and  $F_0(\lambda)$  refers to the extra-atmospheric solar irradiance.

We subsequently obtained Level 1 Landsat series data, geometrically corrected and radiometrically calibrated, from the U.S. Geological Survey website. The Landsat data preprocessing steps included band combination and striping using ENVI 5.3 software.

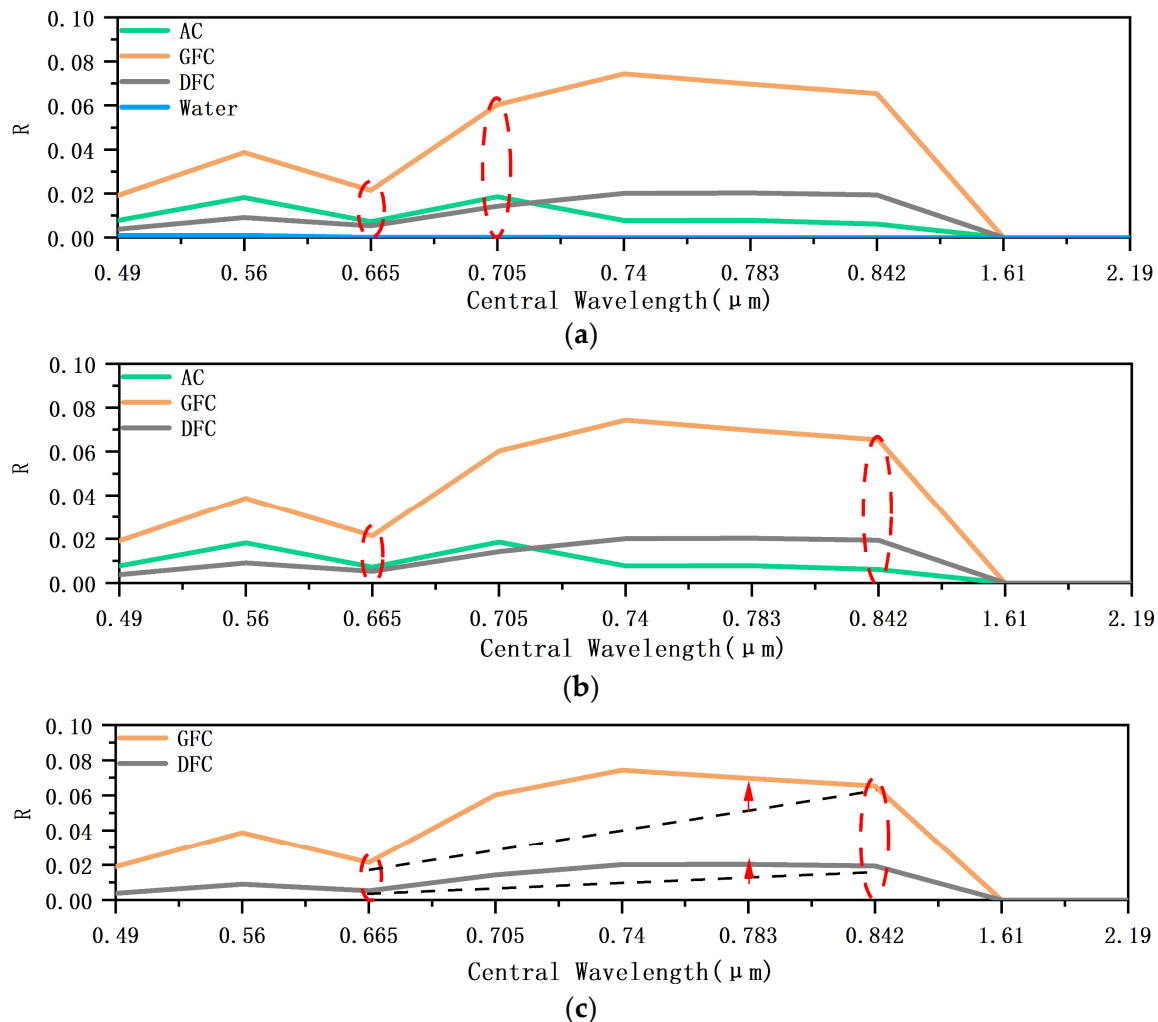
GF PMS image pre-processing involved image fusion and geometric and atmospheric corrections [48].

### 3.2. Classification Decision Tree Model for Three *Cladophora* Morphologies Using Sentinel-2 Data

#### 3.2.1. Spectral Characteristics and Indices Selection

As shown in Figure 4, the reflectance of water gradually approached zero near 0.665  $\mu\text{m}$ . The reflectance spectra of the *Cladophora* in different morphologies resembled those of vegetation at certain wavelengths because of the chlorophyll content. The spectrum contained a reflection peak near 0.56  $\mu\text{m}$ , a valley near 0.665  $\mu\text{m}$ , and a “steep slope effect” in 0.665–0.705  $\mu\text{m}$  [49]. The chlorophyll spectral index (CSI) [50] was used to describe this steep slope, Figure 4a red circles. Specifically, when CSI was below the threshold  $H$ , it was considered water; otherwise, it was *Cladophora*. The CSI was calculated as follows:

$$CSI = \frac{(R_{rs}(0.705) - R_{rs}(0.665))}{(R_{rs}(0.705) + R_{rs}(0.665))} \quad (3)$$



**Figure 4.** Equivalent Reflectance spectrum of AC, GFC, DFC, and water. (a) CSI index used to distinguish *Cladophora* and water; (b) NDVI index used to distinguish AC and FC; (c) FCI index used to identify GFC and DFC.

The reflectance spectrum of AC displayed spectral features of vegetation and water, which resembled those of submerged plants [49]. Owing to the unique physicochemical properties and geographical location of Qinghai Lake, aquatic plants were extremely scarce [29]. When aquatic plants and AC coexist in the lake, they are identified along

with the AC. AC exhibited a downward and an approximate flat trend between 0.665 and 0.842  $\mu\text{m}$  (Figure 4b red circles), whereas the GFC and DFC showed an upward trend from 0.665 to 0.842  $\mu\text{m}$ . The normalized difference vegetation index (NDVI) was used [51,52] to identify AC and FC. If the NDVI was below threshold I, it was AC; otherwise, it was FC (including GFC and DFC). NDVI was calculated as follows:

$$NDVI = \frac{R_{rs}(0.842) - R_{rs}(0.665)}{R_{rs}(0.842) + R_{rs}(0.665)} \quad (4)$$

The GFC reflectance spectrum showed an upward steep slope from 0.665 to 0.74  $\mu\text{m}$  and formed a high reflectivity platform between 0.74 and 0.842  $\mu\text{m}$ . The DFC reflectance spectrum showed a low-reflectivity platform at approximately 0.783  $\mu\text{m}$ . A floating *Cladophora* index (FCI) was applied to separate the GFC and DFC, depending on the difference in the near 0.783  $\mu\text{m}$ . Geometrically, the FCI value can be described as the distance of the red arrow in Figure 4c, which starts from the reflectance of 0.783  $\mu\text{m}$  and ends on the line connecting the reflectance of 0.665  $\mu\text{m}$  and 0.843  $\mu\text{m}$ . If the FCI was below the threshold of J, *Cladophora* was considered DFC; otherwise, it was regarded as GFC. The FCI was calculated as follows:

$$FCI = [R_{rs}(0.783) - R_{rs}(0.665) - ((R_{rs}(0.842) - R_{rs}(0.665))) \times (0.783 - 0.665) / (0.842 - 0.665)] \quad (5)$$

### 3.2.2. Classification Decision Tree Model and Threshold Selection

The CDTM based on Sentinel-2 images consists of four steps (Figure 5). Step 1: using the remote sensing reflectance image generated by pre-processed Sentinel-2 images as the input, the boundary containing *Cladophora* and water is obtained by visual interpretation and image cropping. Step 2: the water and *Cladophora* regions are distinguished by CSI with threshold H. Step 3: the NDVI and threshold I are used to identify *Cladophora* with different morphologies obtaining the AC and FC regions. Step 4: the FCI and threshold J are used to distinguish the GFC and DFC.

Specifically, at the same location directly above AC, another morphology of *Cladophora*, such as GFC or DFC, may simultaneously exist. To avoid situations where *Cladophora* coexists, we simultaneously evaluated the distribution areas of GFC and DFC when calculating the distribution area of AC.

Appropriate thresholds for CDTM are essential for ensuring identification accuracy. The CSI, NDVI, and FCI indices were calculated to distinguish water, AC, GFC, and DFC with in situ reflectance spectral data collected on 87 AC, 106 GFC, 27 DFC, and 87 water in 2020–2022. All of these indices were calculated by in situ measured reflectance in simulated Sentinel-2 bands (Figure 6).

The modelled Sentinel-2 bands of 0.665  $\mu\text{m}$  and 0.705  $\mu\text{m}$  were selected to calculate CSI, and the value with no overlap between the water maximum and the *Cladophora* (AC, GFC, DFC) minimum was chosen as threshold H, about 0, as shown in Figure 6a. Similarly, NDVI and FCI were calculated based on simulated Sentinel-2 bands, with the corresponding indices being selected thresholds I and J, about 0.05 and  $-0.1$ , respectively. The index thresholds were effectively separating categories AC, GFC, and DFC (Figure 6b,c). This study provides thresholds that are all estimates.

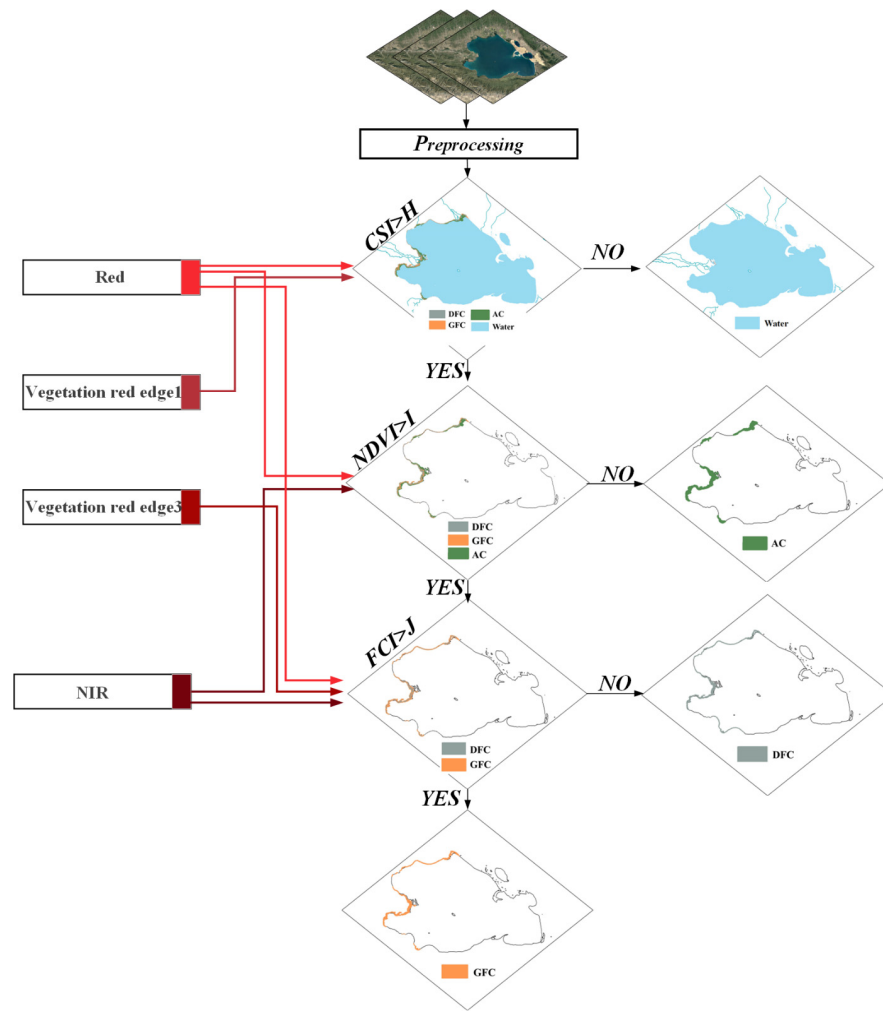


Figure 5. Classification decision tree model for identifying AC, DFC, GFC and water.

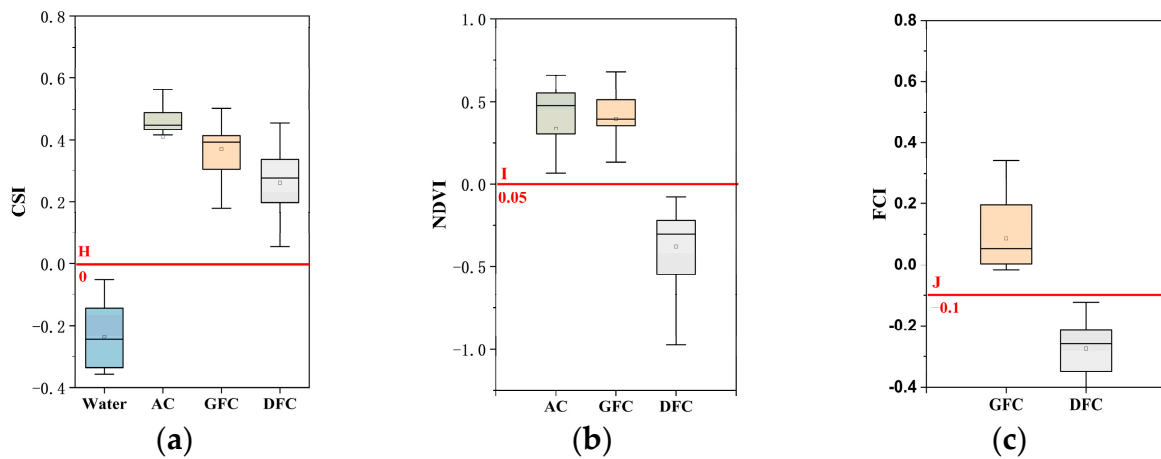


Figure 6. Box-and-whisker plots for threshold selection. (a) CSI and threshold H; (b) NDVI and Threshold I; (c) FCI and threshold J. The solid line in the box represents the median value. The upper and lower box sides represent the 1st and 3rd quartiles (Q1 and Q3), respectively. The upper and lower whiskers represent the maximum and minimum values, respectively.

### 3.3. Visual Interpretation for Two Cladophora Morphologies Using Landsat

The Landsat series satellite images are limited by the sensor’s lack of the two necessary red-edged bands, making it difficult to distinguish the two morphological characteristics

(GFC and DFC) of Floating *Cladophora* (FC). For Landsat series images, we chose not to distinguish between GFC and DFC within the FC, so only floating *Cladophora* (FC) and attached submerged *Cladophora* (AC) were identified. The area of two *Cladophora* morphologies in Landsat satellite images was evaluated using a visual interpretation method that can be used for validation.

We also established, by field experiments, that AC exists below FC in the vertical direction. Therefore, for Landsat series satellite images, FC is included in the AC visual interpretation results (Table 1).

**Table 1.** Criteria for the visual interpretation of *Cladophora* in different areas of Qinghai Lake.

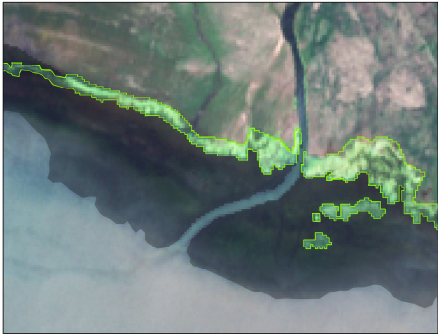





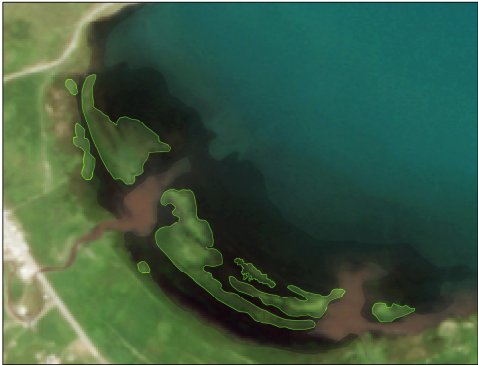
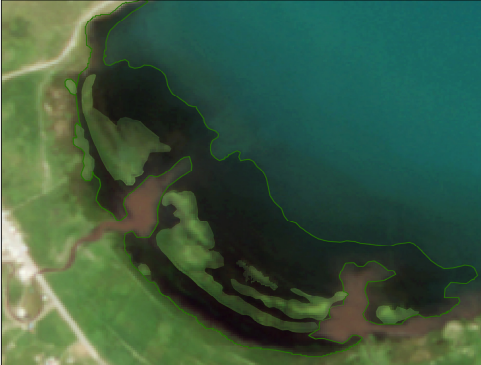
Locations	Floating <i>Cladophora</i> (FC)	Attached Submerged <i>Cladophora</i> (AC)
Characteristics	Shape: Discontinuous distribution in fragmented blocks Spatial distribution: Near the water–land interface of inflowing rivers and lake bays	Shape: Irregular distribution in continuous patches Spatial distribution: Near the water–land interface of inflowing rivers and lake bays
Shaliu River inlet (ROI1)		
Buha River inlet (ROI2)		
Tiebuka Bay (ROI3)		



Table 1. Cont.

Locations	Floating <i>Cladophora</i> (FC)	Attached Submerged <i>Cladophora</i> (AC)
Heima River inlet (ROI4)		

### 3.4. Accuracy Assessment

The accuracy was evaluated by mean relative error (MRE), root mean square error (RMSE) and the average unbiased relative error (AURE) with the following formulae:

$$MRE = \frac{1}{n} \sum_{i=1}^n \frac{|R_i - R_j|}{R_j} \times 100\% \quad (6)$$

$$RMSE = \sqrt{\frac{\sum_{i=1}^n (R_i - R_j)^2}{n}} \quad (7)$$

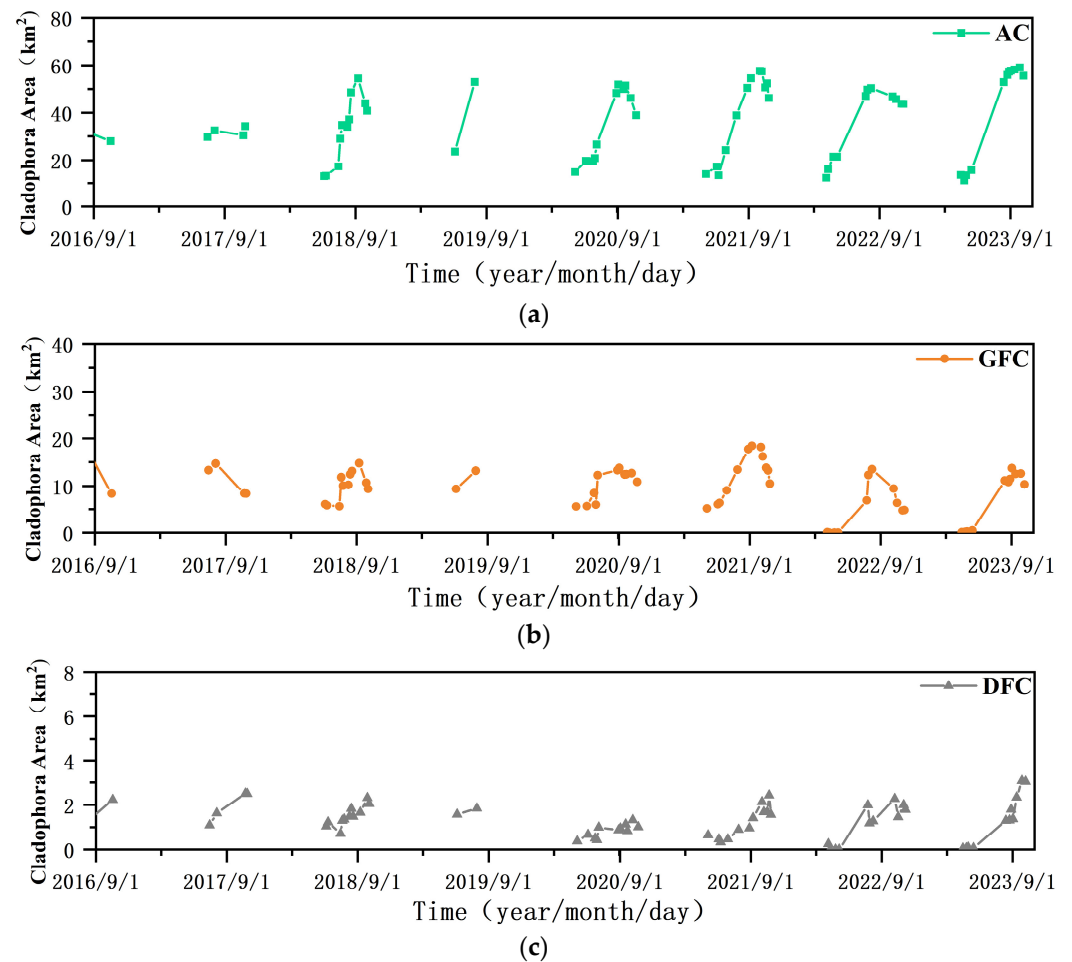
$$AURE = \frac{1}{N} \sum_{i=1}^N \frac{|V_x - V_y|}{(V_x + V_y)/2} \quad (8)$$

where  $n$  represents the number of points;  $R_i$  and  $R_j$  are the predicted and true values, respectively.  $V_x$  and  $V_y$  are the sensor I and sensor II, respectively.

## 4. Results

### 4.1. Interannual Variation Characteristics of Three *Cladophora* Morphologies

In this study, we counted the area distributed by *Cladophora* during the three morphologies of the annual non-ice periods (April to October) from 2016 to 2023. The seasonal variation in areas was similar for the AC, GFC and DFC, as shown in Figure 7. This began annually in May and June, peaked in August and September, and then gradually decreased in October. The AC showed an intra-annual maximum area of approximately 30 km<sup>2</sup> in 2016–2017 and 60 km<sup>2</sup> in 2018–2023. The AC area increased significantly from 2017 to 2018 and then became stable. Compared to the AC area, the GFC area was relatively small and stable, with a maximum of approximately 15 km<sup>2</sup> per year. In 2021, the maximum area suddenly increased to 20 km<sup>2</sup>. Among the areas of the three types of *Cladophora*, the area of DFC was minimal and the least variable. In 2023, the maximum area suddenly increases to 4 km<sup>2</sup>.



**Figure 7.** AC, GFC, and DFC areas obtained by classification decision tree model using Sentinel-2.

#### 4.2. Interannual Spatiotemporal Characteristics of Two Morphologies *Cladophora*

To explore the long-term variation in the different morphologies of *Cladophora*, we utilized various remote sensing data sources, including Sentinel-2 and Landsat series, to obtain information on changes in the two morphologies of *Cladophora* (AC and FC) over an extended period. Over the past 30 years, these morphologies have exhibited a gradual upward trend, and both morphologies have a longstanding history, as shown in Figure 8. Spatially, the two morphologies occurred in most of the shallow near-shore waters of the study area. In particular, the inlet of the Buha River and the area surrounding Bird Island, where AC and FC were aggregated, had the largest area of distribution, followed by the areas of Bay of Tiebuka Lake, the Shaliu River inlet, and the Heima River inlet following. Around 1990, AC and FC areas were approximately 20 km<sup>2</sup> and 7 km<sup>2</sup>, respectively. These areas were lowest during 2005–2011; AC and FC areas were approximately 10 km<sup>2</sup> and 5 km<sup>2</sup>, respectively. This finding matches with the results of previous research [53,54]. After 2011, the *Cladophora* distribution gradually increased, and the AC and FC area increased approximately to 20 km<sup>2</sup> and 10 km<sup>2</sup>, respectively. During 2015–2023, the *Cladophora* area increased annually, with the annual maximum areas distributed by an AC and FC of approximately 60 km<sup>2</sup> and 20 km<sup>2</sup>, respectively. Similar conclusions were reported by Zhu et al. [32].

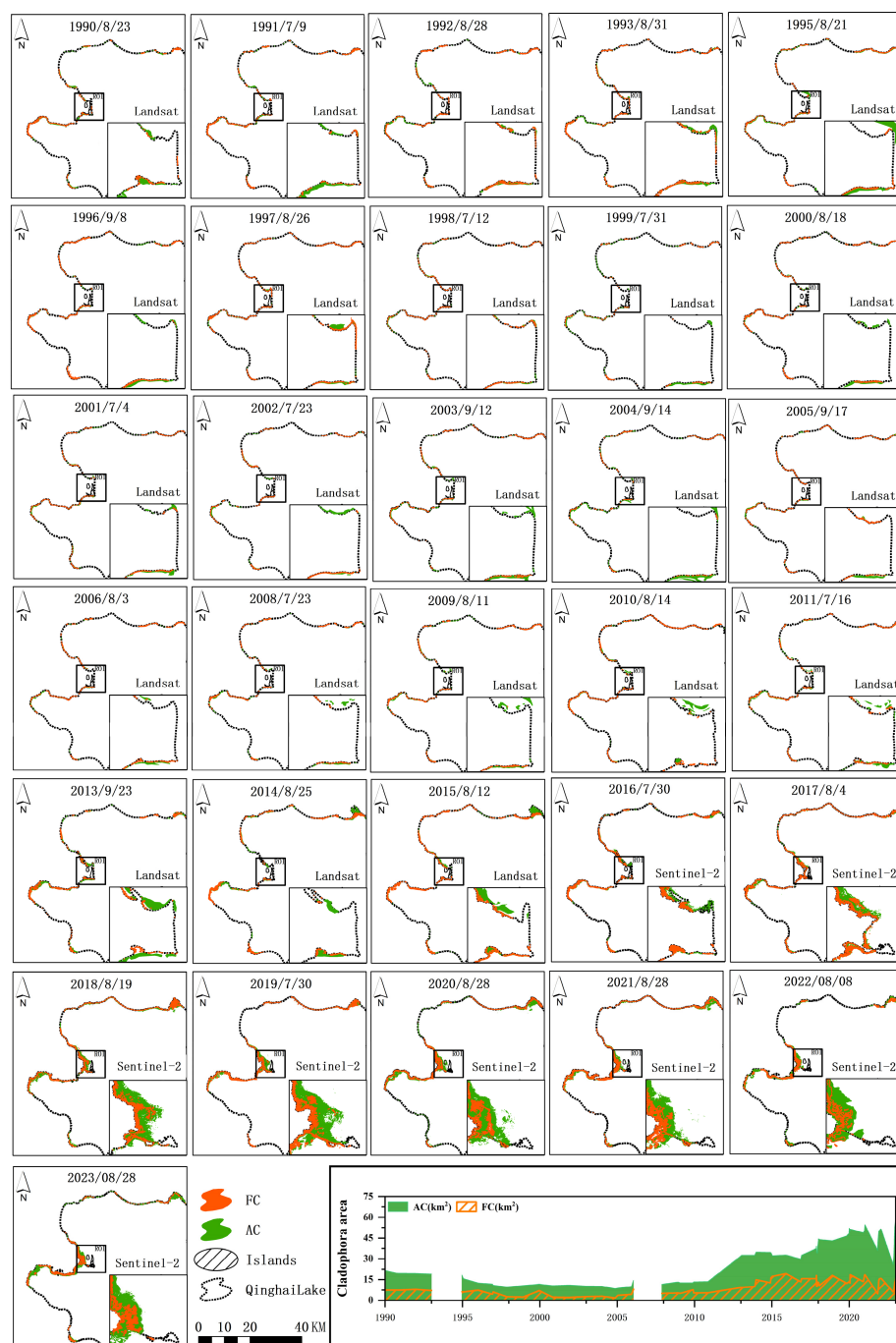


Figure 8. The spatiotemporal distribution of AC and FC.

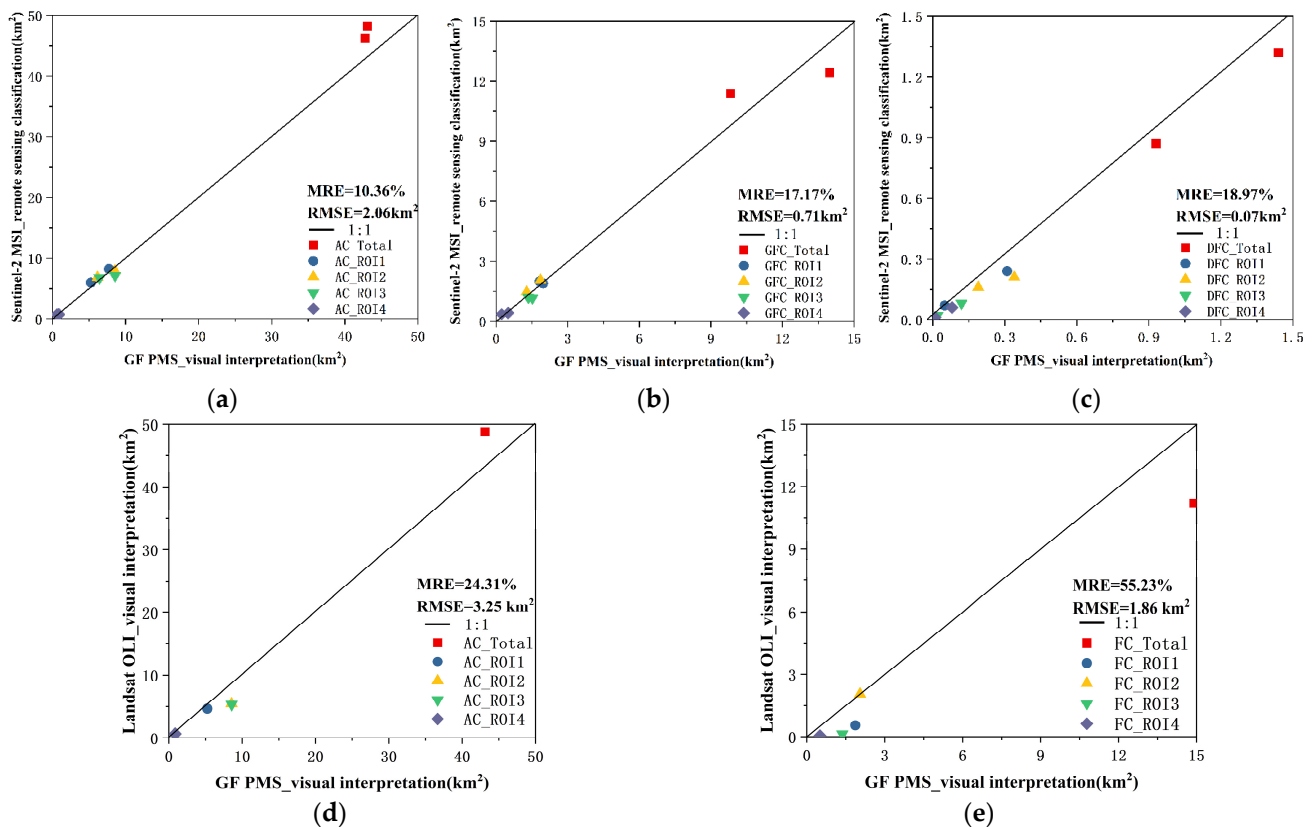
### 4.3. Comparison of Cladophora Classification from Different Remote Sensing Images

#### 4.3.1. Validating the Identification Accuracy of Cladophora Using High Resolution Images

To validate the *Cladophora* identification areas of Sentinel-2 and Landsat OLI images, two quantitative evaluation indicators, RMSE and MRE, were selected. This paper uses the identification areas *Cladophora* in high-resolution remote sensing images GF PMS as nearly the true areas, to describe quantitatively the Sentinel-2 CDTM in identifying three morphologies *Cladophora*, and the Landsat OLI visual interpretation in identifying two morphologies *Cladophora*.

First, to verify the accuracy of the Sentinel-2 CDTM in identifying AC, GFC, and DFC, a total of two periods were selected for comparison of Sentinel-2 and GF PMS images. Specifically, the respective selected dates were 28 August 2020, and 7 October 2020. Owing

to the small number of synchronously collected images, we also selected regions of interest (ROI) 1, 2, 3, and 4 for comparison while comparing the total area of *Cladophora* within the study area (Figure 1). Figure 9 shows the areas obtained by visual interpretation and CDTM, indicating that for the three types of *Cladophora*, the areas obtained by CDTM were consistent with the ground truth data. Specifically, for AC, GFC, and DFC, the MREs were 10.36, 17.17, and 18.97%, respectively, and the RMSEs were 2.06, 0.71, and 0.07 km<sup>2</sup>, respectively. This demonstrates that the proposed CDTM had a high accuracy and could effectively distinguish between AC, GFC, and DFC.



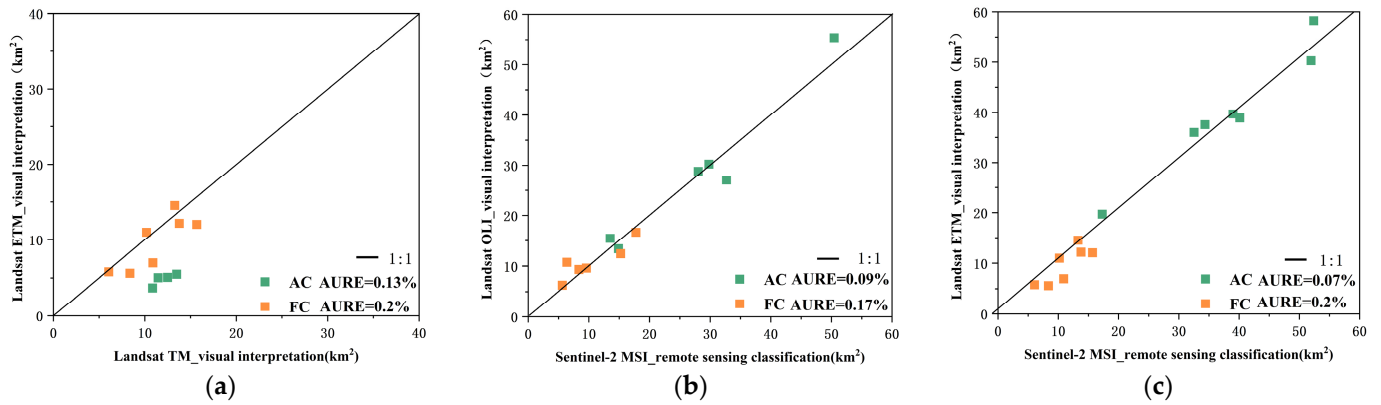
**Figure 9.** Validation of Sentinel-2 MSI and Landsat OLI images for *Cladophora* identification accuracy using high-resolution images (GF PMS). (a) AC area based on Sentinel-2 MSI and GF PMS images. (b) GFC area based on Sentinel-2 MSI and GF PMS images. (c) DFC area based on Sentinel-2 MSI and GF PMS images. (d) AC area based on Landsat OLI and GF PMS images. (e) FC area based on Landsat OLI and GF PMS images.

Secondly, using GF PMS images as the reference data, Landsat images collected on August 25, 2020 with a 30 m resolution were selected for comparison. The MREs of the AC and FC areas were 24.31 and 55.23% and the RMSE values were 3.25 and 1.86 km<sup>2</sup>, respectively.

The distributions of the different morphologies of *Cladophora* were near-identical while the areal differences were minor. This indicates that the two data sources, Sentinel-2 and Landsat, were in close real situations.

#### 4.3.2. Cross-Validating Landsat and Sentinel-2-Based Identification of *Cladophora*

To investigate the consistency of different sensors in identifying the area of *Cladophora*, the AURE was selected as the evaluation indicator to verify the similarity in *Cladophora* identification between different sensors. We cross-validated the following data from different sensors that passed over the same area at nearly the same time: Landsat TM and ETM, Sentinel-2 and Landsat OLI, and Sentinel-2 and ETM (Figure 10).



**Figure 10.** Consistency comparison among different data sources: (a) AC and FC inhabited areas determined based on Landsat TM and ETM images. (b) AC and FC inhabited areas determined based on Sentinel-2 MSI and Landsat OLI images. (c) AC and FC inhabited areas determined based on Sentinel-2 MSI and Landsat ETM images.

To compare the consistency of different sensors in identifying *Cladophora* algae area, Landsat TM and ETM were compared for four groups of images taken eight days apart. The AURE values of the AC and FC areas were 0.13 and 0.2%, respectively. While comparing the identification of AC and FC areas using six-period Sentinel-2 images and Landsat OLI images, the AURE values were 0.09 and 0.17%, respectively. In addition, seven groups of images of Sentinel-2 and Landsat ETM, which were taken within three days, were selected for comparison. The AUREs of AC and FC were 0.07 and 0.2%, respectively.

Overall, there were some differences between various remote sensing data sources in the consistency of identifying algal areas. However, these differences likely did not impact the overall identification results of algae areas significantly.

## 5. Discussion

### 5.1. The Applicability of Classification Decision Tree Model to Other Spectral Indices

In Step 3 of the proposed classification decision tree model, NDVI is used to distinguish AC and FC. To evaluate the applicability of the proposed CDTM when using other spectral indices, this section uses the enhanced vegetation index (EVI) [55], adjusted floating algae index (AFAI) [56], floating algae index (FAI) [19], and virtual-baseline floating algae height (VB-FAH) [9] to identify *Cladophora* instead of NDVI. These indices are calculated as follows:

$$EVI = G \times (R_{rs}(0.842) - R_{rs}(0.665)) / (R_{rs}(0.842) + C_1 \times R_{rs}(0.665) - C_2 \times R_{rs}(0.490) + C_3) \quad (9)$$

$$AFAI = R_{rs}(0.842) - R_{rs}(0.665) + (R_{rs}(1.610) - R_{rs}(0.665)) \times 0.5 \quad (10)$$

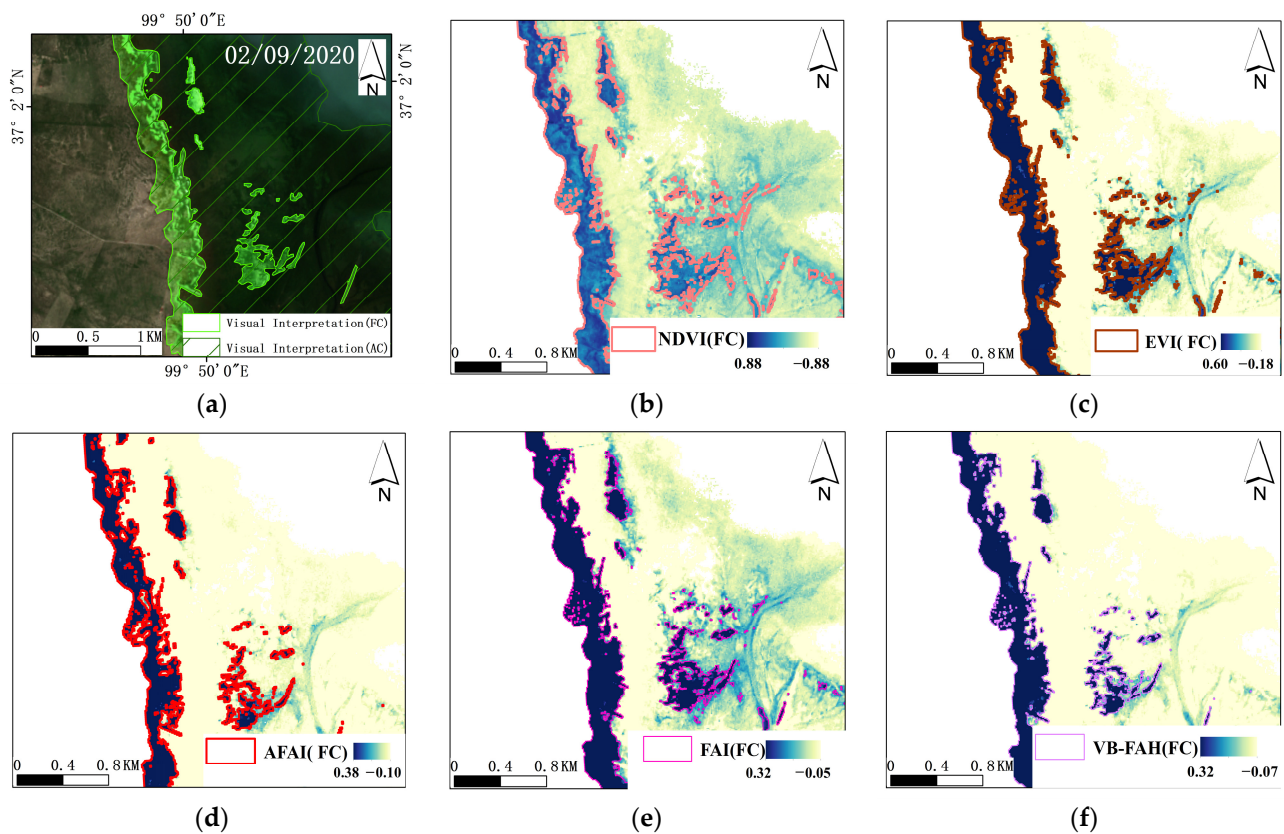
$$FAI = R_{rs}(0.842) - R'_{rs}(0.842) \quad (11)$$

$$R'_{rs}(0.842) = R_{rs}(0.665) + (R_{rs}(1.610) - R_{rs}(0.665)) \times (0.842 - 0.665) / (1.610 - 0.665)$$

$$VB - FAH = (R_{rs}(0.842) - R_{rs}(0.560)) + (R_{rs}(0.560) - R_{rs}(0.665))(0.842 - 0.560) / (2 \times 0.842 - 0.665 - 0.560) \quad (12)$$

where  $G$  is the gain coefficient, with a value of 2.5;  $C_1$ ,  $C_2$ , and  $C_3$  are empirical coefficients with values 2.5, 6, 7.5, and 1, respectively.

Additionally, Sentinel-2 images of 3 September 2020, are selected because of the lack of images on the date of the field experiment (2 September 2020) (Figure 11a). The AC and FC are first identified in steps 1 and 2 of CDTM using other indices. The AC and FC areas obtained by visual interpretation are accurate.



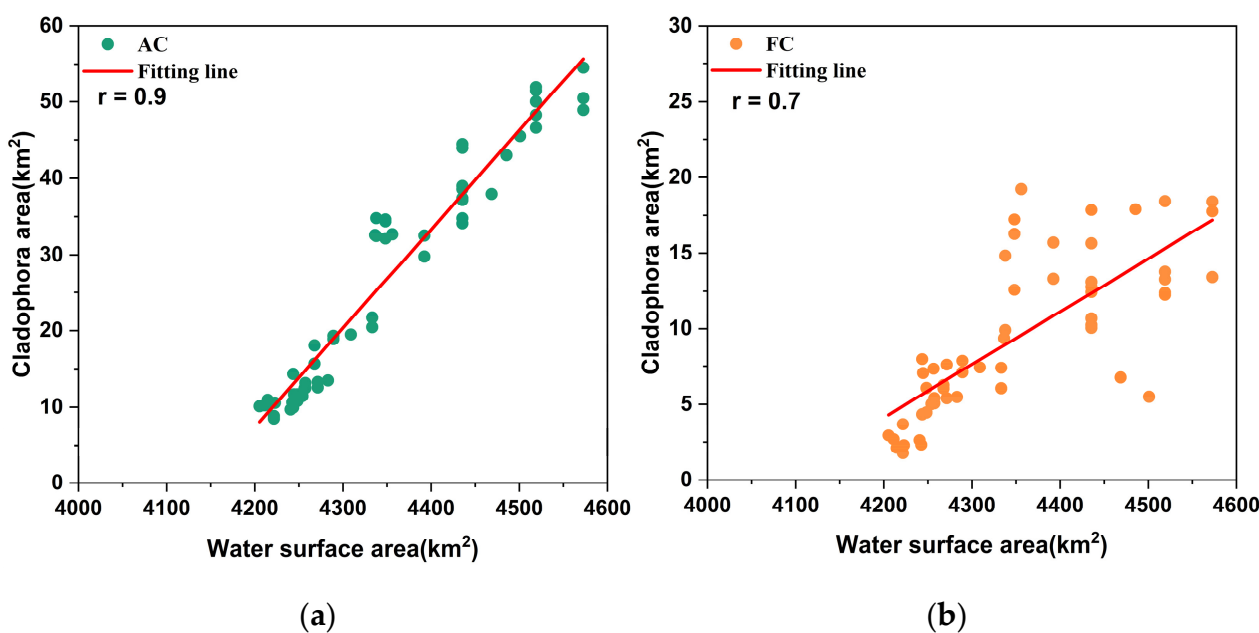
**Figure 11.** The identified AC and FC results by different spectral indices. (a) the field experiment on 2 September 2020, with true color background images from 2 September 2020 Sentinel-2 image; (b) the FC results from NDVI; (c) the FC results from EVI; (d) the FC results from AFAI; (e) the FC results from FAI; and (f) the FC results from VB-FAH.

The results are shown in Figure 11b–f. In comparison, the spectral indices of EVI, AFAI, FAI, and VB-FAH are as effective as NDVI for distinguishing AC and FC. The spatial distribution area obtained by using the above indices is similar to those obtained by using NDVI and is in line with the actual survey. Therefore, all these indices can replace NDVI in this study, and they have the potential to distinguish AC and FC using the proposed CDTM. Using index thresholds to classify submerged macroalgae (AC in this case) is challenging, and more robust models are necessary to improve the accuracy of detection [57]. However, the well-quantified floating macroalgae (FC in this case) in surface water with more reliability showed an increasing trend with the increase in water area of Qinghai Lake (Figure 8).

## 5.2. Analysis of Driving Forces Affecting Changes in *Cladophora*

### 5.2.1. Water Surface Area

This study obtained different morphologies of *Cladophora* (AC and FC) in Qinghai Lake from 1990 to 2023 using visual interpretation and CDTM remote sensing identification methods. Simultaneously, the water surface area of the study region was obtained through visual interpretation. We are surprised that the variation trends of AC and water surface area are highly consistent, the correlation coefficient ( $r$ ) is 0.9, as shown in Figure 12a; this shows the primary factor in the AC variation is water level. FC also exhibited consistency with the variation in water surface area, and  $r$  was 0.7, as shown in Figure 12b, which indicated a certain correlation between FC and water surface area. The result was consistent with those of Wang et al. [44] and Hao et al. [45], who also concluded that FC variations were associated with nutrient inputs from livestock and wildlife drinking, feeding, and defecating, in addition to water surface area factors.



**Figure 12.** The correlation between the water surface area and the *Cladophora* area.

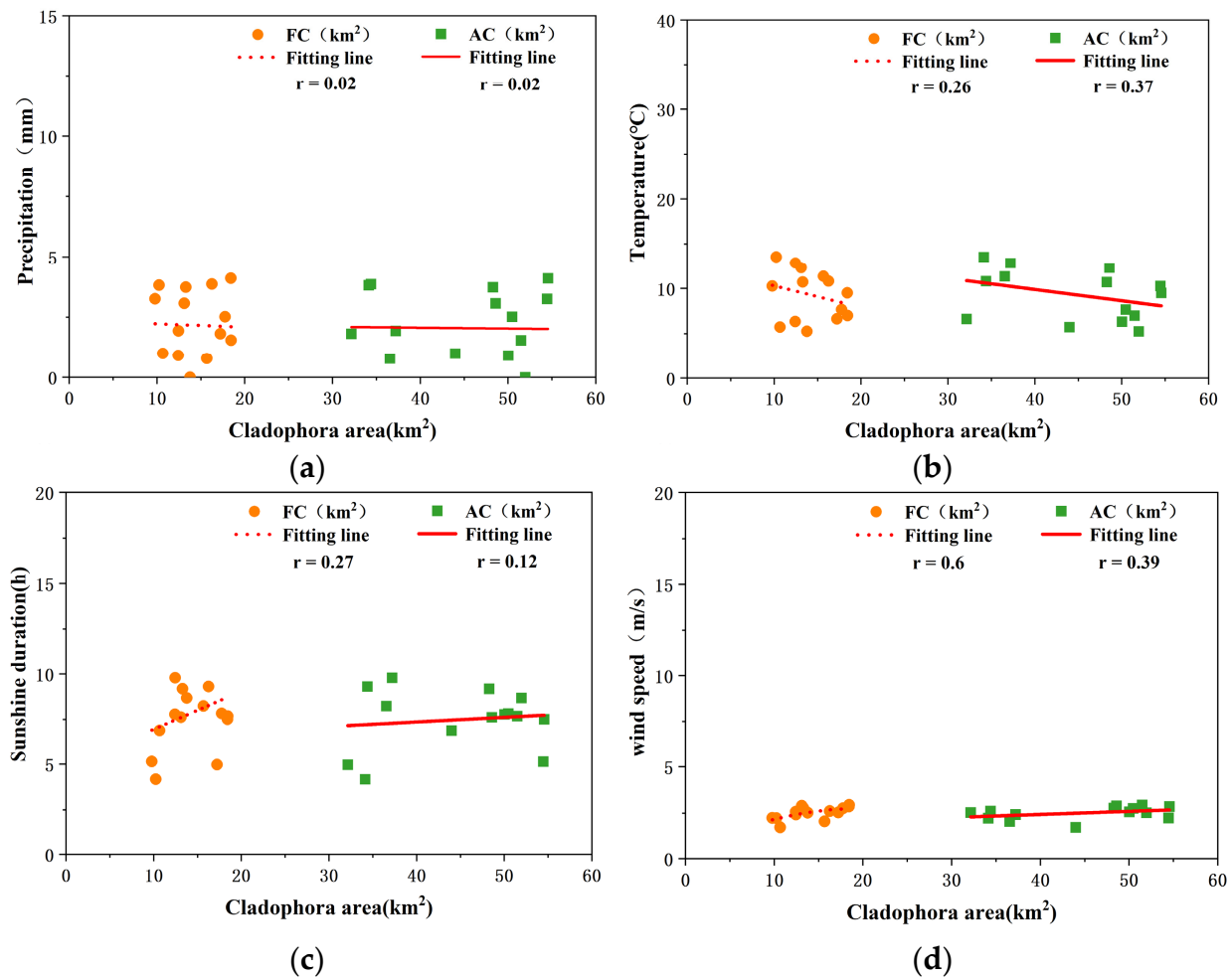
Spatially, we found the area with the most frequent occurrence of *Cladophora* in Bird Island (the area circled in Figure 8) and the area with a large number of waterbirds [58,59]. Spatially, we found that the area of Bird Island (the boxed area in Figure 8), where *Cladophora* frequently occur, greatly overlapped with the area where waterbirds were significantly distributed in Qinghai Lake. Temporally, the seasonal migration time of waterbirds also matches basically with the seasonal growth of *Cladophora*. Therefore, we have reason to hypothesize that in addition to animal husbandry, waterbirds are also promoting the occurrence of *Cladophora*. Waterbirds feeding and inhabiting the site and it accumulates abundant high-phosphorus bird guano. Phosphorus (P) is a nutrient produced by the decomposition of excrements and its facilitation for *Cladophora* growth has been demonstrated in several studies [58,59].

### 5.2.2. Climatic Factors

Climatic factors, including temperature, precipitation, sunshine hours, and wind speed, constitute conditions influencing the regular seasonal variations in *Cladophora*. To explore these influences, the areas of AC and FC were incorporated to determine their correlations with climatic factors. As shown in Figures 7 and 8, large outbreaks of *Cladophora* were observed in the summers (August–September) of 2015–2023. However, the outbreak of *Cladophora* is a process that occurs in different stages, namely, formation, release, attachment, and the death of zoospores [60], among which the formation of zoospores entails an extended timeframe. Hence, data on temperature, precipitation, sunshine duration, and wind speed within a given period (5 days, 7 days, 2 weeks, and 1 month) before the *Cladophora* outbreak were selected. A high correlation was observed between climatic factors and the area of the outbreak 1–5 d prior to the outbreak, which coincided with the growth cycle and seasonal dynamics of the population.

Figure 13 displays the correlation of the selected climatic factors with the respective areas of AC and FC. Both precipitation and sunshine duration had an  $r$  of approximately 0.02–0.27, as shown in Figure 13a,c, demonstrating that precipitation and sunshine duration may not be the primary factors contributing to *Cladophora* outbreaks. In Figure 13b, the temperature, generally correlates with the areas of AC and FC, with  $r$  values of 0.37 and 0.26, respectively. The direct impact of temperature on algal growth and reproduction is determined by the water temperature. Heat from the atmosphere enters the water

body through processes such as convection, conduction, or radiation, influencing water temperature changes, and thus indirectly affecting algal growth [61].



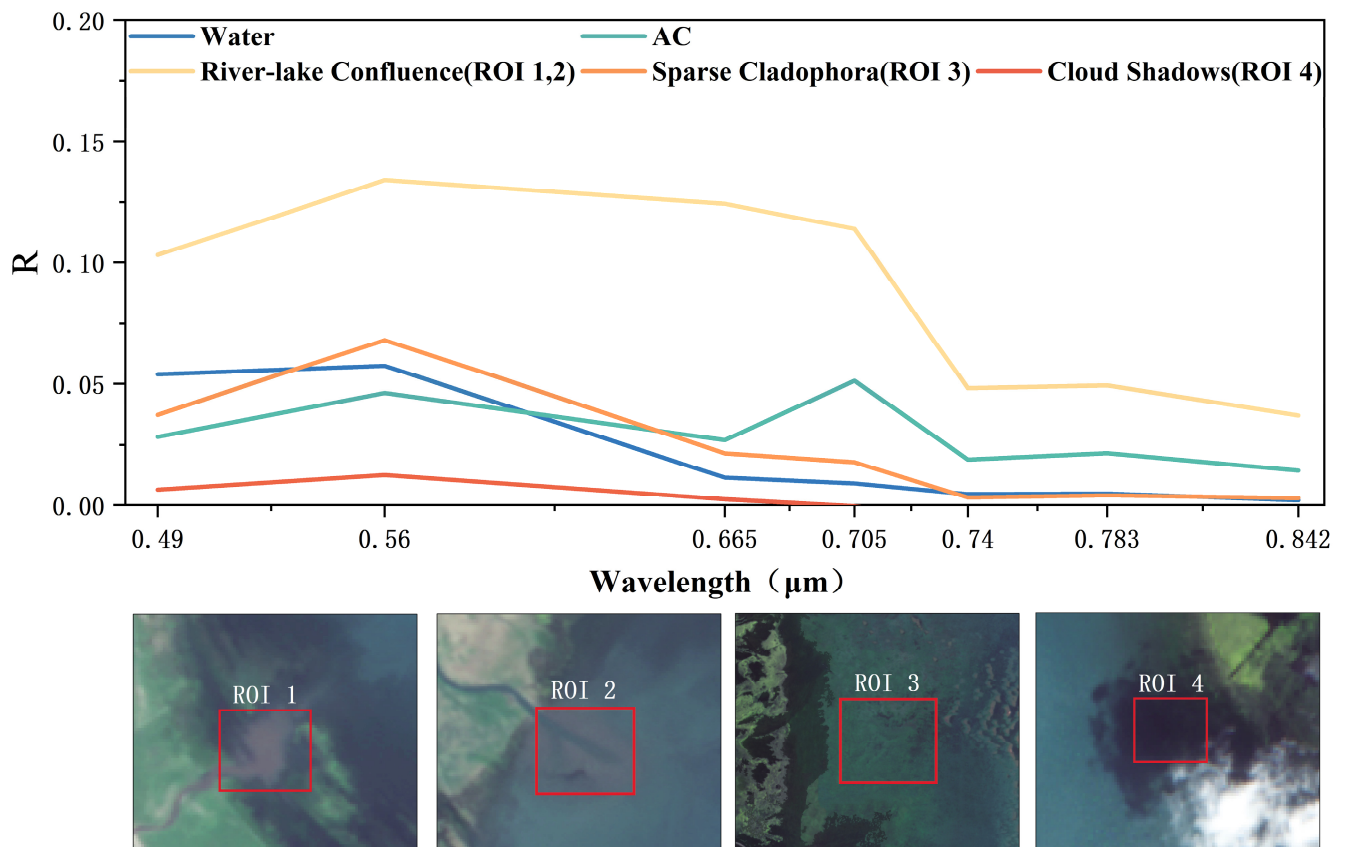
**Figure 13.** The correlation between the climatic factors and the *Cladophora* area. (a) The correlation between precipitation and *Cladophora* area; (b) correlation between temperature and *Cladophora* area; (c) correlation between sunshine duration and *Cladophora* area; and (d) correlation between wind speed and *Cladophora* area.

Furthermore, as shown in Figure 13d, the wind speed is positively correlated with the distribution area of the FC, with an  $r$  value of 0.6. A feasible explanation for this result is as follows: When the wind speed is high, the increased impact force of water flow encourages the expansion of the *Cladophora*, and under the continuous action of wind and waves, the *Cladophora* plants break and float, thereby accelerating the formation of FC.

### 5.3. CDTM Applicability Analysis

When factors such as suspended material, lake bottom substrate, and cloud shadow coincide with *Cladophora* in the shallow waters of Qinghai Lake, the CDTM model demonstrates high applicability. In this study, we extracted reflectance values from Sentinel-2 remote sensing images for various features, including water, AC, areas with high suspended material concentration at river–lake confluence (ROI 1,2), sparse *Cladophora* (ROI 3), and cloud shadows (ROI 4), as shown in Figure 14.





**Figure 14.** CDTM applicability to suspended material, lake bottom, and cloud shadows.

The Qinghai Lake has as a whole clear water, with a transparency ranging from 1.5 to 9.5 m, and a maximum of 10.0 m. The water quality of the lake is very clear. The water reflectance was unaffected by the suspended material. In some specific areas, particularly at the river–lake confluence (ROI 1) and (ROI 2), the influence of inflowing river currents ‘plume’ results in slightly lower transparency in these shallow water compared to the overall of Qinghai Lake. The aforementioned conditions do not affect the CDTM identification of *Cladophora*. The strong hydrodynamics at the river–lake confluence prevent the attachment and growth of *Cladophora*.

Due to the spectral similarity between sparse *Cladophora* (ROI 3) and cloud shadows (ROI 4) with water, this study utilizes the CSI index to directly eliminate features with water-like reflectance characteristics.

## 6. Conclusions

Combining the characteristics of various remote sensing data in identifying *Cladophora*, two sets of remote sensing methods were constructed and utilized to recognize these morphologies. These methods were then applied to long-term remote sensing images to analyze the spatiotemporal distribution and influencing factors of different morphologies of *Cladophora*.

We propose a new classification tree method based on Sentinel-2 images for remote sensing identification of AC, GFC, and DFC areas. The study revealed a seasonal growth pattern for the three morphologies of *Cladophora*, with peak growth in May and June, maximum areas in August and September, and a gradual decline in October.

Furthermore, this study combined Landsat and Sentinel-2 images to analyze the areal changes in two morphologies of *Cladophora* from 1990 to 2023; both showed an increasing trend during this period, thereby demonstrating their longstanding existence. A comparison of *Cladophora* area identification among different sensors, including GF PMS,

Sentinel-2, Landsat TM, ETM, and OLI, revealed minor differences that did not significantly impact the overall results.

Additionally, we analyzed the influence of factors such as water surface area and meteorological elements on the areal changes in different morphologies of *Cladophora*. The results indicate positive correlations between the areas of FC and AC with water surface area, with correlation coefficients ( $r$ ) of 0.7 and 0.9, respectively. The water surface area appeared to be a primary factor influencing *Cladophora* area changes. Furthermore, climatic factors except wind speed had no influence on the growth of *Cladophora*.

In this article, we provide the morphological characteristics of *Cladophora* and its spatio-temporal variations in saltwater lakes, which provides a scientific foundation for further exploring driving factors influencing the different morphologies of *Cladophora*.

**Author Contributions:** Conceptualization, W.X. and Q.S.; project administration, B.Z. and Z.Z.; verification of the results, J.L. and J.S.; supervision, Y.Y.; methodology, Y.Z. and L.L. All authors have read and agreed to the published version of the manuscript.

**Funding:** This research was jointly supported by the National Key Research and Development Program of China (grant number 2021YFB3901101) and the National Natural Science Foundation of China (grant number 41971327).

**Data Availability Statement:** Data available on request from the authors.

**Conflicts of Interest:** The authors declare no conflicts of interest.

## References

- Gower, J.; Hu, C.; Borstad, G.; King, S. Ocean color satellites show extensive lines of floating sargassum in the gulf of Mexico. *IEEE Trans. Geosci. Remote Sens.* **2006**, *44*, 3619–3625. [CrossRef]
- Hu, C.; Lee, Z.; Ma, R.; Yu, K.; Li, D.; Shang, S. Moderate resolution imaging spectroradiometer (MODIS) observations of cyanobacteria blooms in Taihu Lake, China. *J. Geophys. Res. Ocean* **2010**, *115*, C4. [CrossRef]
- Hu, C.; Li, D.; Chen, C.; Ge, J.; Muller-Karger, F.E.; Liu, J.; Yu, F.; He, M.X. On the recurrent *Ulva prolifera* blooms in the Yellow Sea and East China Sea. *J. Geophys. Res. Ocean* **2010**, *115*, C5. [CrossRef]
- Wynne, T.T.; Stumpf, R.P.; Tomlinson, M.C.; Dyble, J. Characterizing a cyanobacterial bloom in western Lake Erie using satellite imagery and meteorological data. *Limnol. Oceanogr.* **2010**, *55*, 2025–2036. [CrossRef]
- Gower, J.; Young, E.; King, S. Satellite images suggest a new Sargassum source region in 2011. *Remote Sens. Lett.* **2013**, *4*, 764–773. [CrossRef]
- Shuchman, R.A.; Sayers, M.J.; Brooks, C.N. Mapping and monitoring the extent of submerged aquatic vegetation in the Laurentian Great Lakes with multi-scale satellite remote sensing. *J. Great Lakes Res.* **2013**, *39*, 78–89. [CrossRef]
- Qi, L.; Hu, C.; Wang, M.; Shang, S.; Wilson, C. Floating Algae Blooms in the East China Sea. *Geophys. Res. Lett.* **2017**, *44*, 11501–11509. [CrossRef]
- Blondeau-Patissier, D.; Brando, V.E.; Lønborg, C.; Leahy, S.M.; Dekker, A.G. Phenology of *Trichodesmium* spp. blooms in the Great Barrier Reef lagoon, Australia, from the ESA-MERIS 10-year mission. *PLoS ONE* **2018**, *13*, e0208010. [CrossRef] [PubMed]
- Xing, Q.; An, D.; Zheng, X.; Wei, Z.; Wang, X.; Li, L.; Tian, L.; Chen, J. Monitoring seaweed aquaculture in the Yellow Sea with multiple sensors for managing the disaster of macroalgal blooms. *Remote Sens. Environ.* **2019**, *231*, 111279. [CrossRef]
- Qi, L.; Tsai, S.F.; Chen, Y.; Le, C.; Hu, C. In Search of Red *Noctiluca scintillans* Blooms in the East China Sea. *Geophys. Res. Lett.* **2019**, *46*, 5997–6004. [CrossRef]
- Zhang, B.; Li, J.; Shen, Q.; Wu, Y.; Zhang, F.; Wang, S.; Yao, Y.; Guo, L.; Yin, Z. Recent research progress on long time series and large scale optical remote sensing of inland water. *Natl. Remote Sens. Bull.* **2021**, *25*, 37–52. [CrossRef]
- Lyons, D.A.; Arvanitidis, C.; Blight, A.J.; Chatzinikolaou, E.; Guy-Haim, T.; Kotta, J.; Orav-Kotta, H.; Queirós, A.M.; Rilov, G.; Somerfield, P.J.; et al. Macroalgal blooms alter community structure and primary productivity in marine ecosystems. *Glob. Chang. Biol.* **2014**, *20*, 2712–2724. [CrossRef]
- Ministry of Science and Technology of China. Ministry of Science and Technology Releases. Annual Report on Global Ecological Environment Remote Sensing Monitoring. 2021. Available online: [http://www.most.gov.cn/kjbgz/202112/t20211222\\_178697.html](http://www.most.gov.cn/kjbgz/202112/t20211222_178697.html) (accessed on 22 December 2021).
- Kutser, T.; Metsamaa, L.; Strömbeck, N.; Vahtmäe, E. Monitoring cyanobacterial blooms by satellite remote sensing. *Estuar. Coast. Shelf Sci.* **2006**, *67*, 303–312. [CrossRef]
- Duan, H.T.; Zhang, S.; Zhang, Y. Cyanobacteria bloom monitoring with remote sensing in Lake Taihu. *J. Lake Sci.* **2008**, *20*, 145–152. [CrossRef]
- Ma, R.; Kong, F.; Duan, H. Spatio-temporal distribution of cyanobacteria blooms based on satellite imageries in Lake Taihu, China. *J. Lake Sci.* **2008**, *20*, 687–694.

17. Gower, J.; King, S.; Goncalves, P. Global monitoring of plankton blooms using MERIS MCI. *Int. J. Remote Sens.* **2008**, *29*, 6209–6216. [[CrossRef](#)]
18. Duan, H.; Ma, R.; Xu, X.; Kong, F.; Zhang, S.; Kong, W.; Hao, J.; Shang, L. Two-decade reconstruction of algal blooms in China's Lake Taihu. *Environ. Sci. Technol.* **2009**, *43*, 3522–3528. [[CrossRef](#)]
19. Hu, C. A novel ocean color index to detect floating algae in the global oceans. *Remote Sens. Environ.* **2009**, *113*, 2118–2129. [[CrossRef](#)]
20. Liu, S.; Yang, M.; Zhang, F.; Zhang, S. Research on early warning of dinoflagellate bloom in Caojie Reservoir base on support vector machine classification. *J. Lake Sci.* **2015**, *27*, 38–43. [[CrossRef](#)]
21. Oyama, Y.; Matsushita, B.; Fukushima, T. Distinguishing surface cyanobacterial blooms and aquatic macrophytes using Landsat/TM and ETM+ shortwave infrared bands. *Remote Sens. Environ.* **2015**, *157*, 35–47. [[CrossRef](#)]
22. Shen, F.; Tang, R.; Sun, X.; Liu, D. Simple methods for satellite identification of algal blooms and species using 10-year time series data from the East China Sea. *Remote Sens. Environ.* **2019**, *235*, 111484. [[CrossRef](#)]
23. Qing, S.; Runa, A.; Shun, B.; Zhao, W.; Bao, Y.; Hao, Y. Distinguishing and mapping of aquatic vegetations and yellow algae bloom with Landsat satellite data in a complex shallow Lake, China during 1986–2018. *Ecol. Indic.* **2020**, *112*, 106073. [[CrossRef](#)]
24. Jin, Y.; Zhang, Y.; Niu, Z.; Jiang, S. Application of Environmental Satellite HJ-1 CCD Data for Cyanobacteria Bloom Remote Sensing in Taihu Lake. *Adm. Tech. Environ. Monit.* **2010**, *22*, 53–56+66. [[CrossRef](#)]
25. Schroeder, S.B.; Dupont, C.; Boyer, L.; Juanes, F.; Costa, M. Passive remote sensing technology for mapping bull kelp (*Nereocystis luetkeana*): A review of techniques and regional case study. *Glob. Ecol. Conserv.* **2019**, *19*, e00683. [[CrossRef](#)]
26. Liu, M.; Ling, H.; Wu, D.; Su, X.; Cao, Z. Sentinel-2 and Landsat-8 observations for harmful algae blooms in a small eutrophic lake. *Remote Sens.* **2021**, *13*, 4479. [[CrossRef](#)]
27. Dai, Y.; Yang, S.; Zhao, D.; Hu, C.; Xu, W.; Anderson, D.M.; Li, Y.; Song, X.-P.; Boyce, D.G.; Feng, L.; et al. Coastal phytoplankton blooms expand and intensify in the 21st century. *Nature* **2023**, *615*, 280–284. [[CrossRef](#)]
28. Zhao, Z.J.; Wang, J.Q.; Zhu, H.; Liu, B.W.; Liu, G.X. *Cladophora rigida* sp. nov., a new freshwater species within *Cladophora* ceae (Ulvophyceae, Chlorophyta) from China. *Phycologia* **2021**, *60*, 164–169. [[CrossRef](#)]
29. Lanzhou Institute of Geology, Chinese Academy of Sciences. *Comprehensive Investigation Report of Qinghai Lake*; Science Press: Beijing, China, 1979; pp. 15–22.
30. Li, S. A preliminary Study on the Types, Evolution and Biological Productivity of Qinghai Lake. In *Proceedings of the Second Plenary Session of the Western Pacific Fisheries Research Commission*; Science Press: Beijing, China, 1959; pp. 97–105.
31. Northwest Institute of Plateau Biology. *Fish Fauna in Qinghai Lake Region and Biology of Gymnocypris przewalskii*; Science Press: Beijing, China, 1975; pp. 44–50.
32. Zhu, H.; Xiong, X.; Ao, H.; Wu, C.; He, Y.; Hu, Z.; Liu, G. *Cladophora* reblooming after half a century: Effect of climate change-induced increases in the water level of the largest lake in Tibetan Plateau. *Environ. Sci. Pollut. Res.* **2020**, *27*, 42175–42181. [[CrossRef](#)] [[PubMed](#)]
33. Duan, H.; Yao, X.; Zhang, D.; Jin, H.; Wei, Q. Long-Term Temporal and Spatial Monitoring of *Cladophora* Blooms in Qinghai Lake Based on Multi-Source Remote Sensing Images. *Remote Sens.* **2022**, *14*, 853. [[CrossRef](#)]
34. Liu, X.; Chen, Y. A review on the ecology of *Cladophora*. *J. Lake Sci.* **2018**, *30*, 881–896. [[CrossRef](#)]
35. Hou, X.; Feng, L.; Chen, X.; Zhang, Y. Dynamics of the wetland vegetation in large lakes of the Yangtze Plain in response to both fertilizer consumption and climatic changes. *ISPRS J. Photogramm. Remote Sens.* **2018**, *141*, 148–160. [[CrossRef](#)]
36. Hou, X.; Feng, L.; Dai, Y.; Hu, C.; Gibson, L.; Tang, J.; Lee, Z.; Wang, Y.; Cai, X.; Zheng, C.; et al. Global mapping reveals increase in lacustrine algal blooms over the past decade. *Nat. Geosci.* **2022**, *15*, 130–134. [[CrossRef](#)]
37. Liang, Q.; Zhang, Y.; Ma, R.; Loisel, S.; Li, J.; Hu, M. A MODIS-based novel method to distinguish surface cyanobacterial scums and aquatic macrophytes in Lake Taihu. *Remote Sens.* **2017**, *9*, 133. [[CrossRef](#)]
38. Shi, H.; Zhang, T.; Li, X.; Niu, Z.C.; Wang, T.T.; Li, Y. Dynamic Monitoring of Distribution of Submerged Vegetation in the North of Taihu Lake in Spring Based on Multi-source Remote Sensing Images. *J. Environ. Monit. Forewarning* **2016**, *8*, 13–18.
39. Yang, J.; Luo, J.; Lu, L.; Sun, Z.; Cao, Z.; Zeng, Q.; Mao, Z. Changes in aquatic vegetation communities based on satellite images before and after pen aquaculture removal in East Lake Taihu. *J. Lake Sci.* **2021**, *33*, 507–517. [[CrossRef](#)]
40. Sagan, V.; Peterson, K.T.; Maimaitijiang, M.; Sidike, P.; Sloan, J.; Greeling, B.A.; Maalouf, S.; Adams, C. Monitoring inland water quality using remote sensing: Potential and limitations of spectral indices, bio-optical simulations, machine learning, and cloud computing. *Earth Sci. Rev.* **2020**, *205*, 103187. [[CrossRef](#)]
41. Xiong, Y.; Ran, Y.; Zhao, S.; Zhao, H.; Tian, Q. Remotely assessing and monitoring coastal and inland water quality in China: Progress, challenges and outlook. *Crit. Rev. Environ. Sci. Technol.* **2020**, *50*, 1266–1302. [[CrossRef](#)]
42. Ghosh, A.; Subudhi, B.N.; Bruzzone, L. Integration of Gibbs Markov random field and hopfield-type neural networks for unsupervised change detection in remotely sensed multitemporal images. *IEEE Trans. Image Process.* **2013**, *22*, 3087–3096. [[CrossRef](#)] [[PubMed](#)]
43. He, C.; Shi, P.; Xie, D.; Zhao, Y. Improving the normalized difference built-up index to map urban built-up areas using a semiautomatic segmentation approach. *Remote Sens. Lett.* **2010**, *1*, 213–221. [[CrossRef](#)]
44. Wang, T.C.; Lu, L.H.; Liu, G.X. Analysis of lakeside wetland evolution and driving factors around Qinghai Lake. *J. China Inst. Water Resour. Hydropower Res.* **2020**, *18*, 274–283. [[CrossRef](#)]

45. Hao, M.; Zhu, H.; Xiong, X.; He, Y.; Ao, H.; Yu, G.; Wu, C.; Liu, G.; Luo, Z.; Liu, J.; et al. Analysis on the distribution and origin of *Cladophora* in the nearshore water of Qing Hai Lake. *J. Acta Hydrobiol. Sin.* **2020**, *44*, 1152–1158. [[CrossRef](#)]
46. Wang, Y.; Zhou, P.; Zhou, W.; Huang, S.; Peng, C.; Li, D.; Li, G. Network Analysis Indicates Microbial Assemblage Differences in Life Stages of *Cladophora*. *Appl. Environ. Microbiol.* **2023**, *89*, e0211222. [[CrossRef](#)] [[PubMed](#)]
47. Zhang, L. A Dissertation Submitted to Wuhan University of Technology for the Doctor's Degree in Engineering. *Wuhan Univ. Technol.* **2019**. [[CrossRef](#)]
48. Shen, Q.; Yao, Y.; Li, L.W.; Long, T.F.; Chen, F.; Zhang, B. Annual 0.8 m surface reflectance data set of Beijing plain area from 2015 to 2019. *Natl. Remote Sens. Bull.* **2021**, *25*, 2303–2312. [[CrossRef](#)]
49. Zhang, B.; Li, J.; Wang, Q.; Sheng, Q. *Hyperspectral Remote Sensing of Inland Water*; Science Press: Beijing, China, 2012; pp. 208–210.
50. Li, J.; Wu, D.; Wu, Y.; Liu, H.; Shen, Q.; Zhang, H. Identification of algae-bloom and aquatic macrophytes in Lake Taihu from in-situ measured spectra data. *J. Lake Sci.* **2009**, *21*, 215–222. [[CrossRef](#)]
51. Rouse, J.W.; Haas, R.H.; Schell, J.A.; Deering, D.W. Monitoring vegetation systems in the great plains with ERTS. *NASA Spec. Publ.* **1974**, *351*, 309–317.
52. Zhang, D.; Xun, Y.; Bao, S.; Ding, Y.; Dong, L.; Huang, L.; Zhao, J.; Gao, Y. Using multi-source satellite imagery data to monitor cyanobacterial blooms of Chaohu Lake. *Infrared Laser Eng.* **2019**, *48*, 726004. [[CrossRef](#)]
53. Yao, W.; Shi, J.Q.; Qi, H.F.; Yang, J.X.; Jia, L.; Pu, J. Study on the phytoplankton in Qinghai Lake during summer of 2006–2010. *Freshw. Fish.* **2011**, *41*, 22–28. [[CrossRef](#)]
54. Yao, W.C. Study on Summer Bait Biological Resources in Qinghai Lake. Ph.D. Thesis, Southwest University, Chongqing, China, 2011. [[CrossRef](#)]
55. Huete, A.; Didan, K.; Miura, T.; Rodriguez, E.P.; Gao, X.; Ferreira, L.G. Overview of the radiometric and biophysical performance of the MODIS vegetation indices. *Inorganica Chim. Acta* **2002**, *83*, 195–213. [[CrossRef](#)]
56. Fang, C.; Song, K.S.; Shang, Y.X.; Ma, J.H.; Wen, Z.D.; Du, J. Remote sensing of harmful algal blooms variability for lake Hulun using adjusted FAI (AFAI) algorithm. *J. Environ. Inform.* **2019**, *34*, 108–122. [[CrossRef](#)]
57. Xing, Q.; Liu, H.; Li, J.; Hou, Y.; Meng, M.; Liu, C. A Novel Approach of Monitoring *Ulva pertusa* Green Tide on the Basis of UAV and Deep Learning. *Water* **2023**, *15*, 3080. [[CrossRef](#)]
58. Zhang, G.; Liu, D.; Jiang, H.; Hou, Y.; Dai, M.; Chu, G. Population Status of Waterbirds in Qinghai Lake After the Occurrence of Avian Influenza. *J. Zool.* **2008**, *2*, 51–56. [[CrossRef](#)]
59. Hou, Y.; He, Y.; Xing, Z.; Cui, P.; Yin, Z.; Lei, F. Diversity and Distribution of Waterbirds in Qinghai Lake National Nature Reserve. *Acta Zool. Sin.* **2009**, *34*, 184–187.
60. Hoffmann, J.P.; Graham, L.E. Effects of selected physicochemical factors on growth and zoosporogenesis of *Cladophora glomerata* (Chlorophyta). *J. Phycol.* **1984**, *20*, 1–7. [[CrossRef](#)]
61. Yang, S.; Jin, W.; Wang, S.; Hao, X.; Yan, Y.; Zhang, M.; Zheng, B. Chlorophyll ratio analysis of the responses of algae communities to light intensity in spring and summer in Lake Erhai. *Environ. Earth Sci.* **2015**, *74*, 3877–3885. [[CrossRef](#)]

**Disclaimer/Publisher's Note:** The statements, opinions and data contained in all publications are solely those of the individual author(s) and contributor(s) and not of MDPI and/or the editor(s). MDPI and/or the editor(s) disclaim responsibility for any injury to people or property resulting from any ideas, methods, instructions or products referred to in the content.